BRAZILIAN JOURNAL OF PETROLEUM AND GAS
Journal Homepage: www.portalabpg.org.br/bjpg
A publication of the ABPG BRAZILIAN ASSOCIATION OF R&D IN PETROLEUM AND GAS

WATER-OIL SEPARATION PROCESS USING A CONCENTRIC TUBULAR CERAMIC MEMBRANE MODULE: A NUMERICAL INVESTIGATION

[a] Cunha, A. L. [1]; [b] Farias Neto, S. R.; [c] Lima, A. G. B.; [c] Barbosa, E. S.; [a] Santos, J. P. L.; [a] Silva, G. F.

[a] Center of Exact Sciences and Technology, NUPETRO, Federal University of Sergipe, Aracajú, SE, Brazil
[b] Center of Science and Technology, DEQ, Federal University of Campina Grande, Campina Grande, PB, Brazil
[c] Center of Science and Technology, DEM, Federal University of Campina Grande, Campina Grande, PB, Brazil

Received: 17.08.2016 / Revised: 03.11.2016 / Accepted: 07.11.2016 / Published on line: 29.12.2016

ABSTRACT

In the present work, it was developed a numerical study on separation processes using ceramic membranes. The study apparatus consisted of a separation module formed by four concentric tubes, where the most inner one corresponds to the ceramic membrane. The system was applied to the treatment of oil and water mixtures. The separation module had a tangential effluent input and a tangential concentrate output. The filtered fluid was collected inside the membrane after filtration. The numerical study used a 3-D computational domain, and it was executed by means of the commercial software ANSYS CFX 12. In the numerical test, the porosity of the membrane was considered as a constant and the permeability as a function of the resistance of the porous media to the flow. At last, it were presented and analyzed the results for pressure, velocity, oil concentration distribution inside the device, permeation velocity, and pressure profiles at the surface of the membrane. The numerical results obtained indicate that the mathematical model used was capable of predicting the deposition of the oil at the surface of the tubular membrane. A geometric analysis of the separation module, supported by the system operation conditions, showed an important influence of this parameter on the dispersion of the concentration polarization at the surface of the equipment. The results showed that the geometric aspects of the proposed microfiltration module and the membrane distribution within the separation module had a significant influence on the hydrodynamic flow leading to polarized layer dispersion.

KEYWORDS

numerical simulation; turbulent flow; ceramic membrane; concentration polarization; CFX

---

[1] To whom all correspondence should be addressed.
Address: Center of Exact Sciences and Technology, Federal University of Sergipe, NUPETRO, Aracajú, SE, Brazil | ZIP Code: 49100-000 | e-mail: actolimacunha@yahoo.com.br
doi:10.5419/bjpg2016-0017

1. INTRODUCTION

The main function of a porous membrane is to separate soluble components from solutions based on the size, charge, shape, and molecular interactions between solute and membrane surface. This feature has attracted the interest of researchers and engineers for decades. In the 1950's, studies showed for the first time the technical and economic viability of the membrane separation processes applied to water desalination by reverse osmosis. The interest in the subject has increased considerably. Improving selectivity and reducing transport resistance of the permeating species represent changes that can make the membrane separation processes more competitive. These benefits can be observed not only in water desalination processes, but also in traditional separation processes such as settling tanks, floaters, two-phase/three-phase separators, and hydrocyclones **(Habert et al., 2006)**. In membrane separation processes, the concentration polarization and fouling formation are phenomena that must be controlled and minimized, because they reduce the permeate flow and can affect product quality. The concentration polarization is a reversible phenomenon that occurs in the first minutes of filtration, resulting in an increase in the concentration of retained species near the membrane surface. Establishing a concentration gradient causes an additional resistance to mass transfer, leading to a decreased permeate flow **(Baker, 2004; Habert et al., 2006; Kulkarni et al., 1992; Song, 1998)**.

Cunha et al. (2013) applied a two-dimensional mathematical model whose numerical solutions of the Navier-Stokes equations are coupled to the Darcy law at the mass transfer analysis along the tubular membrane surface. They evaluated the effect of several physical parameters on concentration profiles and boundary layer thickness, which had lower values with increasing axial Reynolds and Schmidt numbers, as observed by **Damak et al. (2004a)**, **Pak et al. (2008)**, and **Paris et al. (2002)**. They also observed that increasing the axial Reynolds number leaded to an increase in system pressure, which in turn caused an increase in transmembrane pressure, resulting in a higher solute concentration at the membrane surface.

In evaluating the effects of turbulent flow on the membrane separation process, **Zimmerer and Kottke (1996)** analyzed the effects of spacers in the mixture, and found that the spacer “design” may increase turbulence and liquid instability. **Vieira et al. (2012)** evaluated the effect of the geometric aspect on the three-dimensional behavior of the streamlines. They added a tubular device forming an annular space within the microfiltration module, which enabled the presence of a swirling flow. This addition led to a higher filtrate volume.

Yuanfa et al. (2009) performed a numerical study on the turbulent flow of calcium carbonate suspensions to verify the effect of different baffles in the flow pattern and mass transfer at the membrane’s surface. The authors observed that the increase in flow due to intense velocity fluctuations and shear stress in the wall hindered the development of the boundary layer, preventing the growth of the cake layer. They observed that the pressure drop along the tubular membrane is increased significantly due to the frequent changes in flow direction and energy dissipation of turbulent flow caused by baffles matrix.

The behavior of the polarized layer and the formation of fouling are related closely to mass transfer and hydrodynamics in membrane modules. The improvement in flow hydrodynamics can be achieved through changes in module configuration, such as presence of instabilities like baffles or corrugated regions, turbulent regimes and pulsed flow. These strategies allow the decrease in polarization layer next to the membrane surface, improving the permeate flow **(Agarwal and Kaur, 2002; Baker, 2004; Belfort, 1989)**.

One of the biggest technological obstacles involving the membrane separation process is related with the decrease in permeate flow due to the opposition to the transmembrane flow appearing at the surface (concentration polarization, gel layer) and within the porous media (blocking pores, adsorption, and membrane resistance) during the microfiltration process, being the phenomenon of the concentration polarization one of main agents that reduce the permeate flow. Concerned with these problems, the aim of this work is to study the hydrodynamic influence of the flow on the reduction of the concentration polarization formed at the membrane surface. It was analyzed a water-oil

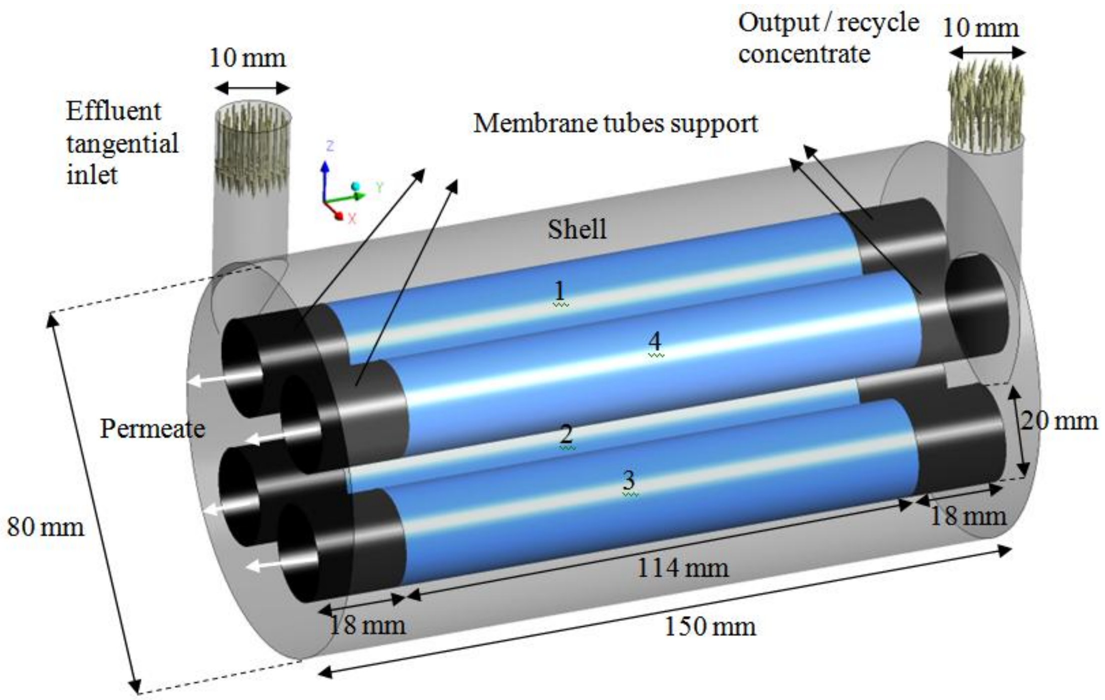

Figure 1. Effluent separation device with tangential inlet containing four membranes.

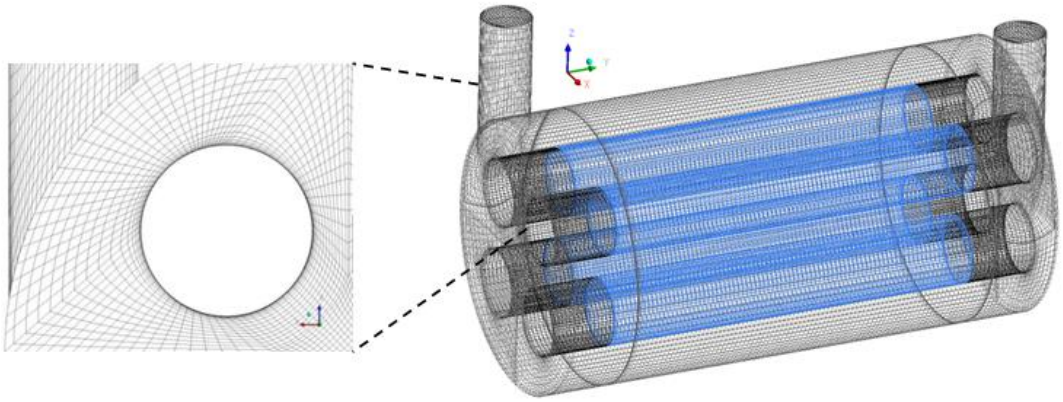

Figure 2. Three-dimensional structured mesh of the microfiltration module containing four membranes.

mixture flowing in the shell-and-tube separation module, into which tubular ceramic membranes were inserted.

2. METHODOLOGY

2.1Problem description

A separation module was designed based on a shell-and-tube radiator, which consists of a large pipe enwrapping four tubular ceramic membranes with the same diameter, responsible for the microfiltration process. This module is provided with tangential inlet and outlet, as illustrated in Figure 1. The dimensions of the shell-and-tube separation module are also represented in Figure 1.

The membranes were arranged within the module so that the distance between their centers was equal to 28.28 mm, being equally distanced from the shell. Figure 2 depicts the numerical mesh of the shell-and-tubes separation module containing four membranes. It consists of 761,705 hexahedral elements and 798,901 nodes.

2.2Mathematical Modeling

The mathematical model used to describe the fluid flow within the device and in the porous medium corresponds to a generalization of the mass and momentum conservation equations (Navier-Stokes equations), and a mass transport equation. The Navier-Stokes equations represent a group of equations that describe the motion of fluid substances and establish that changes in acceleration and momentum of a fluid particle are simply due to pressure variations and dissipative viscous forces (similar to friction) acting within the fluid. In this situation, it is assumed that:

- The flow is considered to be turbulent and at a steady state;
- The solute diffusion coefficient is considered to be constant;
- The gravitational effect is negligible;
- The viscosity and density of the fluids are constant;
- The fluid is incompressible;
- There is no slip condition at the membrane surface, device wall, and membrane connection tubes;
- The wall permeation rate is determined based on the resistance-in-series model;
- The solute does not obstruct the pores of the porous medium;
- No reaction or adsorption of oil occurs at the porous media contact surface;
- The resistance is due to the concentration layer in fluid-membrane interface (concentration polarization resistance).

In the membrane-based separation process, several factors may cause the reduction of the permeate flow, such as blockage of the pores, adsorption, formation of a gel layer, resistance of the membrane itself; and, specially, the formation of a polarized layer. During the simulations, it was considered the resistance of the membrane and the polarized layer, neglecting the other factors. This, however, does not jeopardize the analysis of the membrane separation process, since the settling of oil on the surface of the membrane is the main phenomenon that causes the reduction of permeate flow.

Then, considering the assumptions above, the mass (Eq. 1), momentum conservation (Eq. 2), and mass transfer (Eq. 4) equations can be written as follows:

- Mass conservation:

$$\nabla \bullet (\rho \vec{U}) = 0 \tag{1}$$

Where ρ is the specific mass and $\vec{U}$ is the velocity vector.

- Momentum conservation:

$$\nabla \bullet (\rho \vec{U} \otimes \vec{U}) - \nabla \bullet (\mu_{ef} \nabla \vec{U}) = \\ = -\nabla p + \nabla \bullet (\mu_{ef} (\nabla \vec{U})^T) \tag{2}$$

Where *p* is the pressure and μ_{ef} corresponds to effective viscosity, defined by Equation (3):

$$\mu_{ef} = \mu + \mu_t \tag{3}$$

Where μ is the dynamic viscosity and μ_t is the turbulent viscosity.

- Mass transport equation:

$$\vec{U} \bullet \nabla C = D_{ab} \nabla^2 C \tag{4}$$

Where *C* represents the oil concentration and D_{ab} is the mass diffusivity.

2.2.1 Turbulence model

The shear stress transport (SST) turbulence model was used in the simulation. It proved to be more complete when studying the phenomenon of turbulent flow based on the fact that the pressure and concentration gradient are steeper near the fluid-solid interface. Near the fluid-membrane interface, the flow is described by the k-ϖ model, which is already in the solution. In the case where the k-ϖ model is not able to provide satisfactory results, the k-ε model is applied according to the solution requirement.

There are two transport equations in the SST model, being one equation for the turbulent kinetic energy (*k*), Equation (5), and one for the turbulent frequency (ϖ modified), Equation (6).

$$\frac{\partial(\rho k)}{\partial t}+\nabla\bullet(\rho\vec{U}\,k)=\nabla\bullet\left[(\mu+\frac{\mu_t}{\sigma_{k2}})\nabla k\right]+ \qquad (5)$$

$$+P_k-\beta^{'}\rho k\varpi$$

$$\frac{\partial(\rho\varpi)}{\partial t}+\nabla\bullet(\rho\vec{U}\,\varpi)=\nabla\bullet\left[(\mu+\frac{\mu_t}{\sigma_{\varpi2}})\nabla\varpi\right]+ \qquad (6)$$

$$+(1-F_1)2\rho\frac{1}{\sigma_{\varpi2}\varpi}\nabla k\nabla\varpi+\alpha_2\frac{\varpi}{k}P_k-\beta_2\rho\varpi^2$$

Being:

$$F_1=\tanh(\arg_1) \qquad (7)$$

$$\arg_1=\min\left[\max\left(\frac{\sqrt{k}}{\beta^{'}\varpi y},\frac{500\nu}{y^2\varpi}\right),\frac{4\rho k}{CD_{k\varpi}\sigma_{\varpi2}y^2}\right] \qquad (8)$$

$$CD_{k\varpi}=\max\left(2\rho\frac{1}{\sigma_{\varpi_2}\varpi}\nabla k\nabla\varpi,\ 1.0x10^{-10}\right) \qquad (9)$$

Where y is the closest distance to the wall and ν is the kinematic viscosity. The values of some new constants that appear in the equations above are show below:

$$\alpha_2=0.44 \qquad (10)$$

$$\beta_2=0.0828 \qquad (11)$$

$$\sigma_{k2}=1 \qquad (12)$$

$$\sigma_{\varpi_2}=1/0.856 \qquad (13)$$

These constants have little theoretical footing and are a result of numerous data fitting iterations for a wide range of turbulent flows obtained through the comparison with experimental results in the process of fine-tuning the model. This way, the SST model provides very good calculations for wall bounded flows even with highly separated regions.

Behavior of the transport can be achieved by limiting the formulation of the eddy viscosity (ν_t) by Equation (14) and (15):

$$\nu_t=\frac{a_1k}{\max(a_1\varpi,S\,F_2)} \qquad (14)$$

$$\nu_t=\frac{\mu_t}{\rho} \qquad (15)$$

Where F_2 is a combination function (Eq .16) similar to F_1, which determines the limit on the wall boundary layer. *S* is an invariant measure of the shear rate tensor. The combinations of functions are critical to the success of the method. Its formulation is based on the closest distance to the surface and on the variables of the flow as follows.

$$F_2=\tanh(\arg_2^2) \qquad (16)$$

$$\arg_2=\max\left(\frac{2\sqrt{k}}{\beta^{'}\varpi y},\frac{500\nu}{y^2\varpi}\right) \qquad (17)$$

2.2.2 Initial and boundary conditions

As can be seen in Figure 3, it was adopted a pre-established flow rate condition (Q) at the effluent inlet and a pre-established pressure condition (P_{ext}) at the concentrate output. No slip condition is assumed at the membrane surface, device shell wall and membrane connections tube.

At the membrane wall (tube porous wall), it was assumed that the slip condition were not valid (axial velocity on the wall equal to zero). Neglecting the influence of the local roughness, due to the wall porous nature, one has:

$$U_y=0 \qquad (18)$$

Through the porous wall, the radial velocity U_z is equal to the permeation rate U_w, so that:

$$U_z=U_w \qquad (19)$$

Inside the membrane, it was assumed that there was no accumulation of particles in the steady state – almost 100 % of the particles were rejected by the membrane. Therefore, one can write:

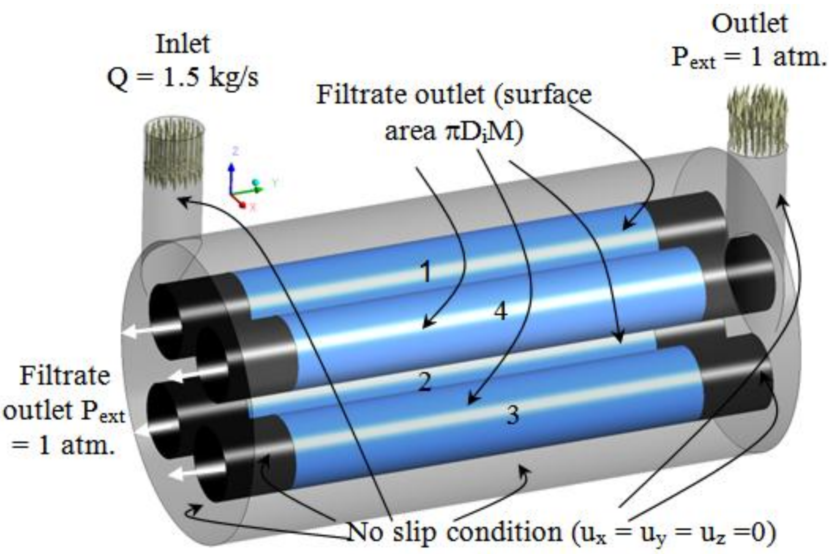

Figure 3. Three-dimensional simulation conditions used in the separation module.

$$U_w C = D\frac{\partial C}{\partial y} \quad (20)$$

The local permeation rate U_w given by Darcy's law, written as the resistance-in-series model, was implemented as a source term in the output boundary condition of the permeate, as follows:

$$U_w = \frac{\Delta P}{\mu(R_m + R_p)} \quad (21)$$

Where ΔP is the transmembrane pressure, defined as the difference between the average pressure at the fluid-membrane interface ($\bar{P}$) and the pressure outside the membrane (P_{ext}). R_m corresponds to the hydraulic resistance of the membrane, given by:

$$R_m = \frac{\text{Membrane thickness}}{\text{Membrane permeability}} \quad (22)$$

To study the behavior of the microfiltration process inside a module containing tubular ceramic membranes, simulations were performed considering the operating conditions, as reported in Table 1.

The specific resistance of the polarized layer (R_p), the permeability of the porous medium (k), the feed concentration (C_0), and the diffusion coefficient (D_{ab}) were kept constant.

Other important data that were defined in the solution of the problem are the properties of the fluids and those of the porous medium. Since the solution was highly diluted, its physical and chemical properties matched those of water. These properties are listed in Table 2.

Table 1. Conditions applied to the simulation.

C_0 / (kg m^{-3})	μ / (Pa.s)	k / m^2	Q / (kg/s)	R_p / (m^{-1})	D_{ab} / (m^2 s^{-1})	R_m / (m^{-1})
1.0	1.1	$1 \cdot 10^{-8}$	1.5	$2.5 \cdot 10^{-8}$	$1.0 \cdot 10^{-9}$	$3.0 \cdot 10^{8}$

Table 2. Physical and chemical properties of the fluid and the membrane.

Water/Oil	Dynamic viscosity	50 cP
	Molar mass	18.02 kg/kmol
	Density	997 kg/m^3
Membrane	Porosity	0.35

3. RESULTS AND DISCUSSIONS

Concerning the shell-and-tubes module, it were evaluated permeate flow, transmembrane pressure, streamlines, velocity vector field, distribution of oil concentration in the separation module, and pressure field. The simulations were performed considering turbulent flow.

The analysis of fluid dynamics inside the shell-and-tubes module can be verified by the streamlines in the separation module, as shown in Figure 4. There is clearly a turbulent fluid flow between the device shell and the membrane surface facing the shell (Figure 4a); and a turbulent behavior of the fluid in the center, between the membranes (Figure 4b). This was expected due to the positioning of the membranes, which are located in the central region of the module. The membranes act as obstacles, breaking the swirling motion of the flow as it crashes into the membrane. There is a reduction in the fluid flow rate in the region located between the membranes.

The results shown in Figure 4 highlight the changes in the behavior of the streamlines at the surface of the membranes due to the injection of permeate into the wall of the porous membrane. On the membrane face turned to the shell, the streamlines follow the turbulent behavior described above, flowing along the surface of the membrane towards the central region (between the membranes). From this position, the axial momentum becomes dominant instead of the angular momentum, provoked by the flow changes caused by the membranes, as seen in Figures 5 (a) and (b).

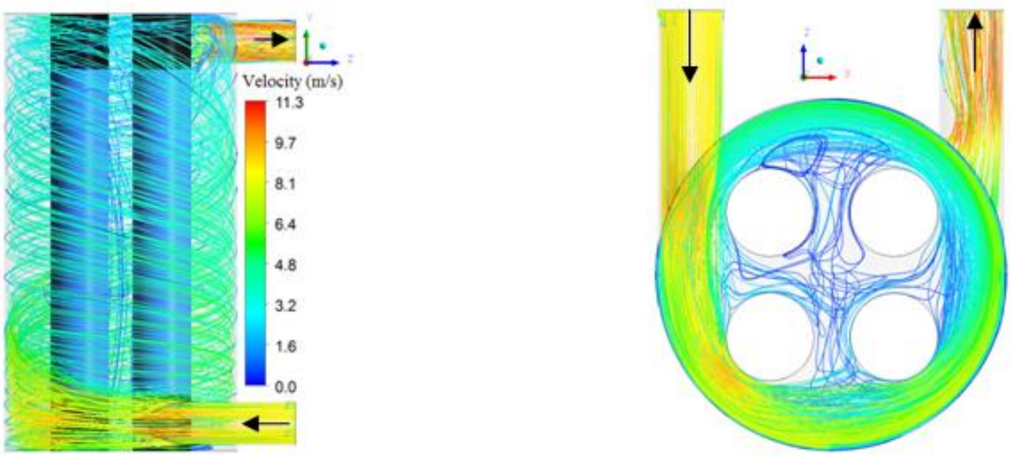

(a) (b)

Figure 4. Streamline inside the shell-and-tubes module: (a) axial view and (b) radial view.

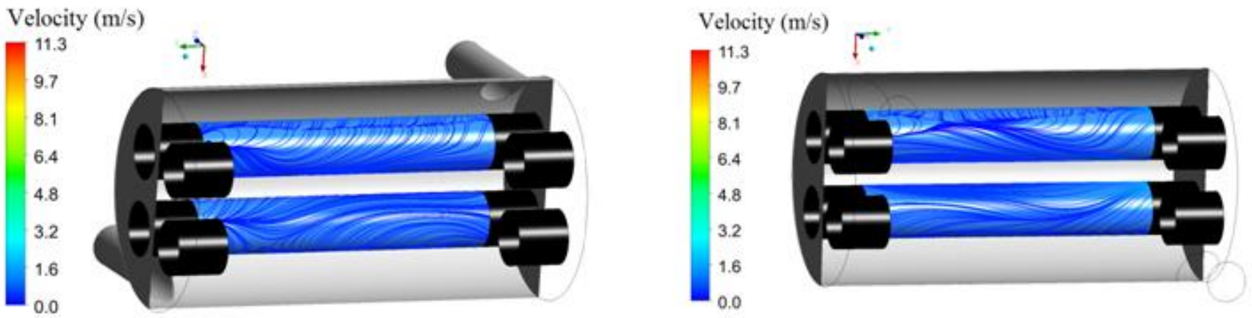

(a) (b)

Figure 5. Streamlines at the membranes.

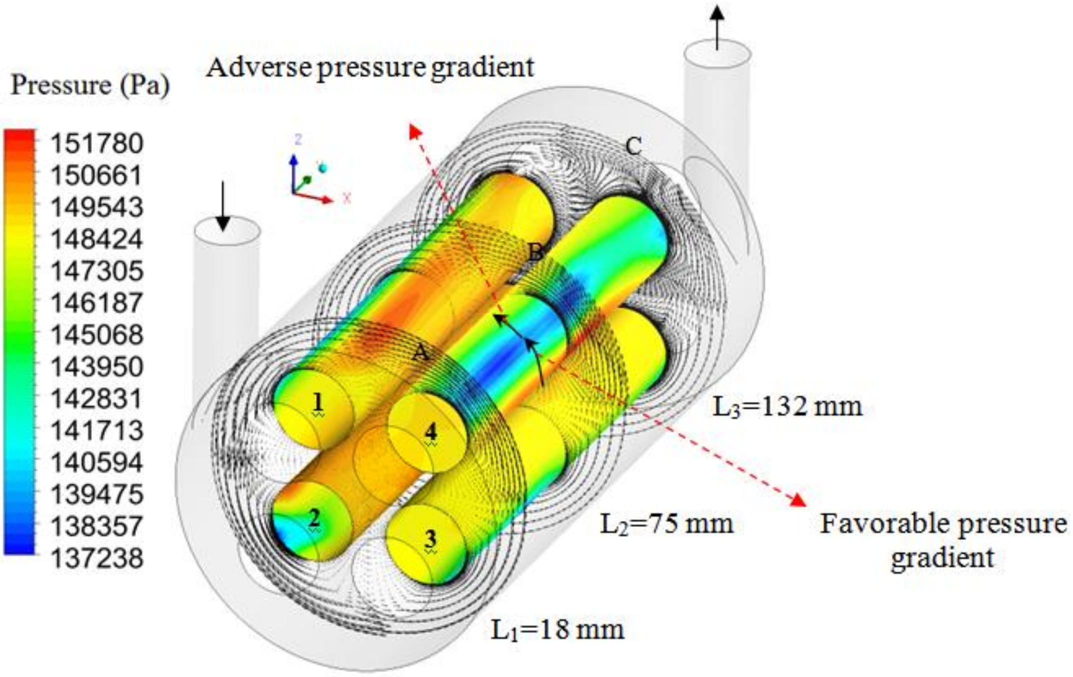

Figure 6. Pressure field on the membrane walls and velocity vector field on planes A, B, and C.

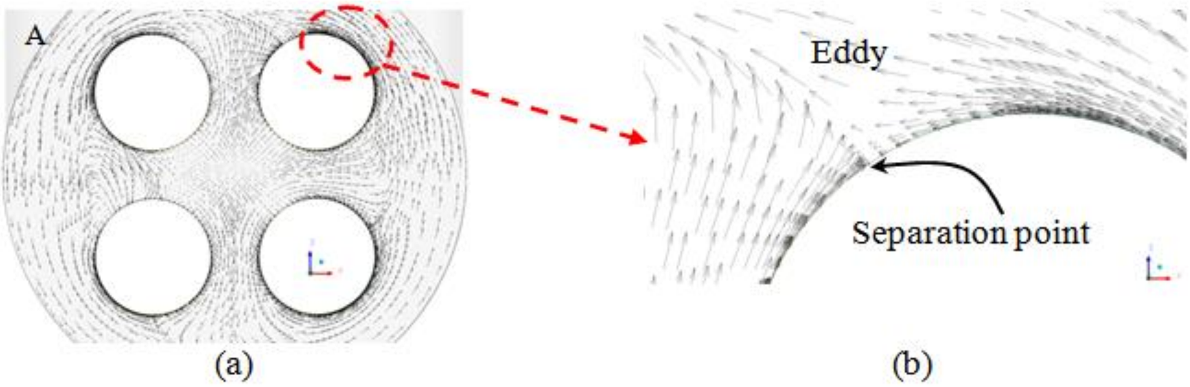

Figure 7. Velocity vector field on plane A (a), and details of the separation of the boundary layer at the surface of the membrane (b).

Figure 6 illustrates the pressure field at the surface of the membranes, as well as the velocity vector field on three transverse planes A, B, and C. One may observe that the fluid hydrodynamic behavior in the inner part of the shell-and-tubes module generates regions with both favorable and adverse pressure gradients. The hydrodynamic boundary layer develops on the surface of the membrane, under the influence of a favorable pressure gradient. However, at some point, the pressure reaches a minimum value (blue region on the membranes surface) and, in the face opposite to the minimum pressure region, the development of the boundary layer occurs in the presence of an adverse pressure gradient, with the separation of the boundary layer from the surface of the membrane, as shown in detail in Figures 7-9. In these figures, the velocity vector fields are represented on planes A, B, and C, respectively. Figure 10 shows the angular positions and also the numbering of membranes.

In Figures 11-14, the pressure profiles are shown in four angular positions (0, 90, 180, and 270°) for each membrane, according to what is proposed in Figure 10 for the angular positions and numbering of the membranes. In these Figures, one can notice that the pressure fields exhibit maximum pressure regions, in which the fluid is flowing between the shell and the membrane

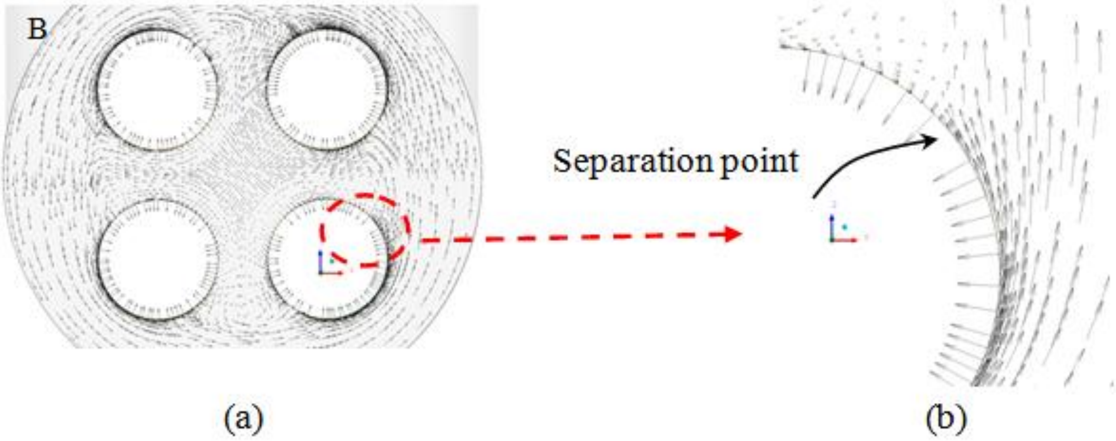

Figure 8. Velocity vector field on plane B (a), and details of the boundary layer separation on the membrane surface (b).

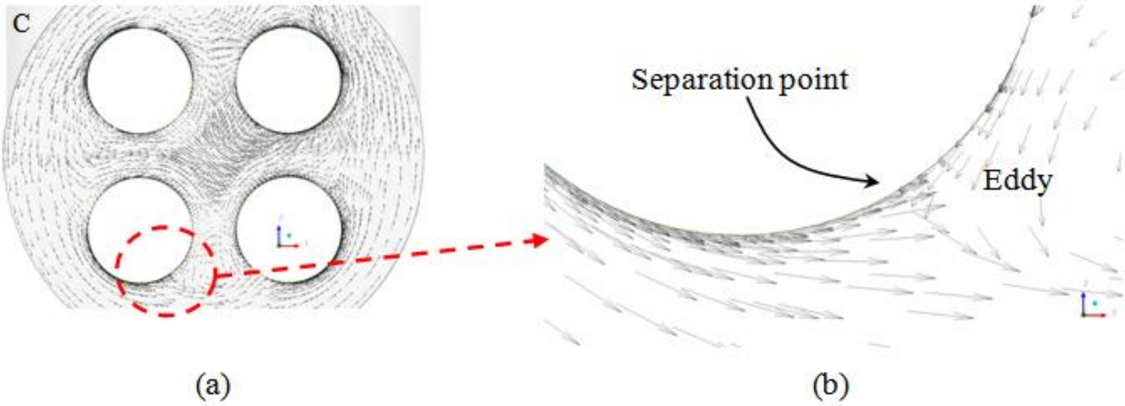

Figure 9. Velocity vector field on plane C (a), and details of the boundary layer separation on the membrane surface (b).

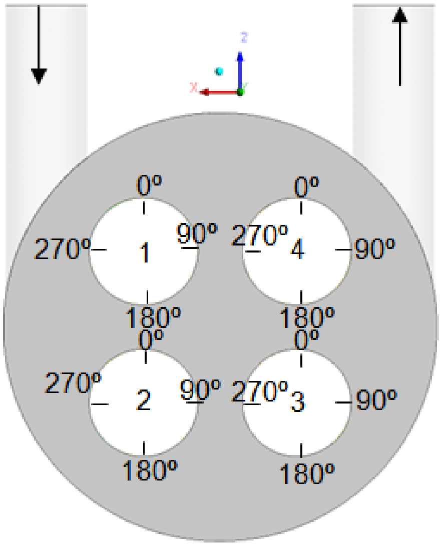

Figure 10. Angular positions and numbering of the membranes.

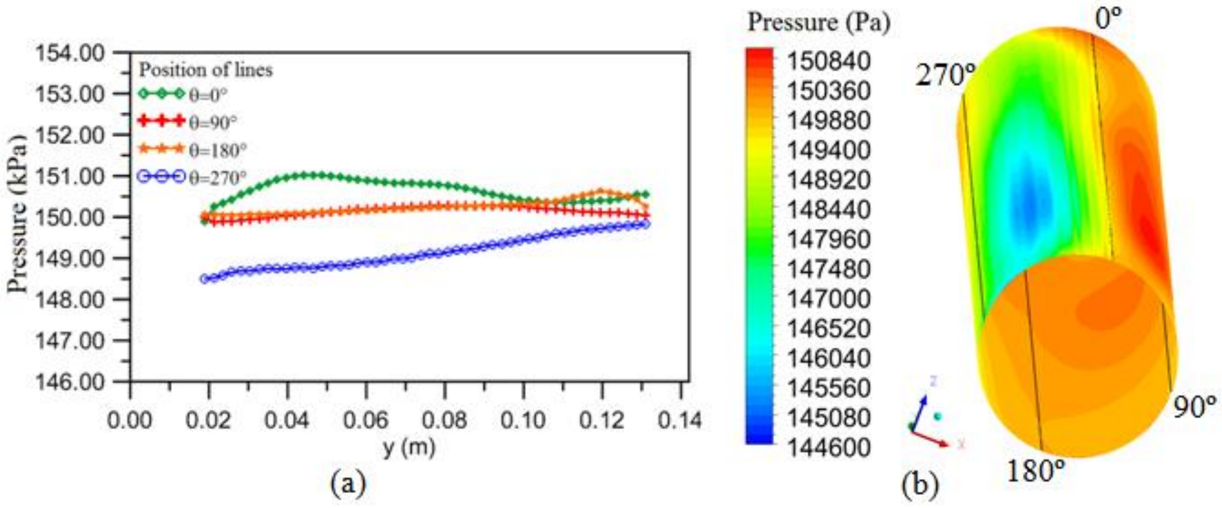

Figure 11. Pressure profiles (a) and pressure field (b) on the wall of membrane 1.

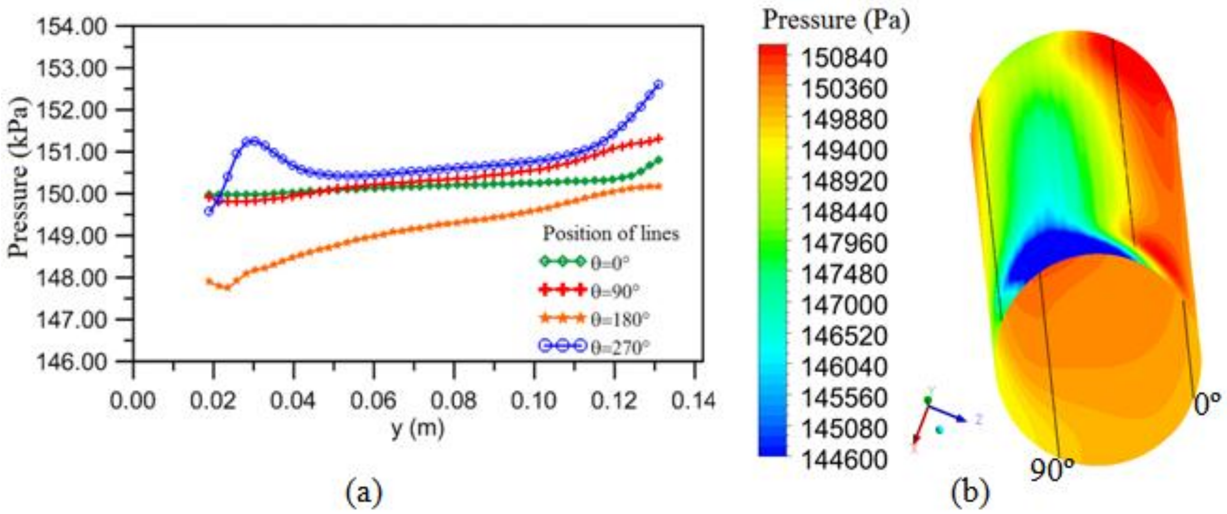

Figure 12. Pressure profiles (a) and pressure field (b) on the wall of membrane 2.

surface facing the shell, hitting the surface of the membrane, followed by regions of reduced pressure. This pressure variation is called favorable pressure gradient. Downstream the minimum pressure section, velocity decreases (Figure 12) and pressure increases (adverse pressure gradient). Due to the loss of momentum, the fluid does not return to its original configuration. It possibly reaches a rest condition, reversing its direction, causing the phenomenon of the separation of the boundary layer, in which it is separated from the body surface, forming a vortex, as observed in Figures 7 to 9.

From the pressure profile, it is possible to observe the reduction of the pressure between the angular positions 0° and 270° for membrane 1, between 270° and 180° for membrane 2, between 180° and 90° for membrane 3, and between 90° and 0° for membrane 4, which corresponds to the membrane side facing the shell, as illustrated in Figure 10.

Figure 15 shows the velocity fields on the transverse planes A, B, and C in the separation module. It must be pointed out that there is a region with high velocity, located between the shell and the membrane surface facing the shell, and a region with low velocity, located in the region between the membranes. Observing the detail of

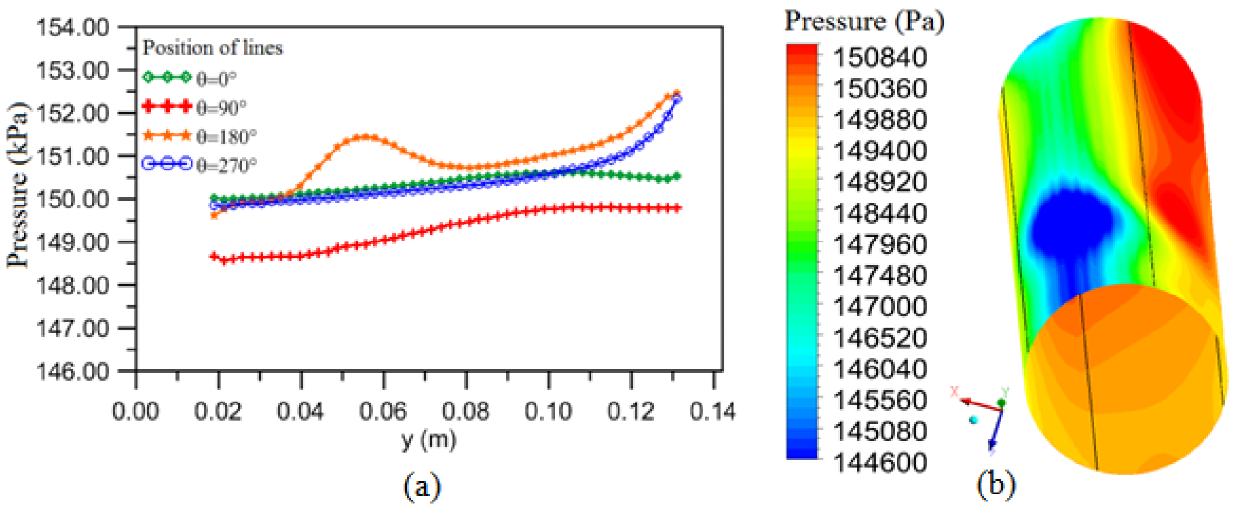

Figure 13. Pressure profiles (a) and pressure field (b) on the wall of membrane 3.

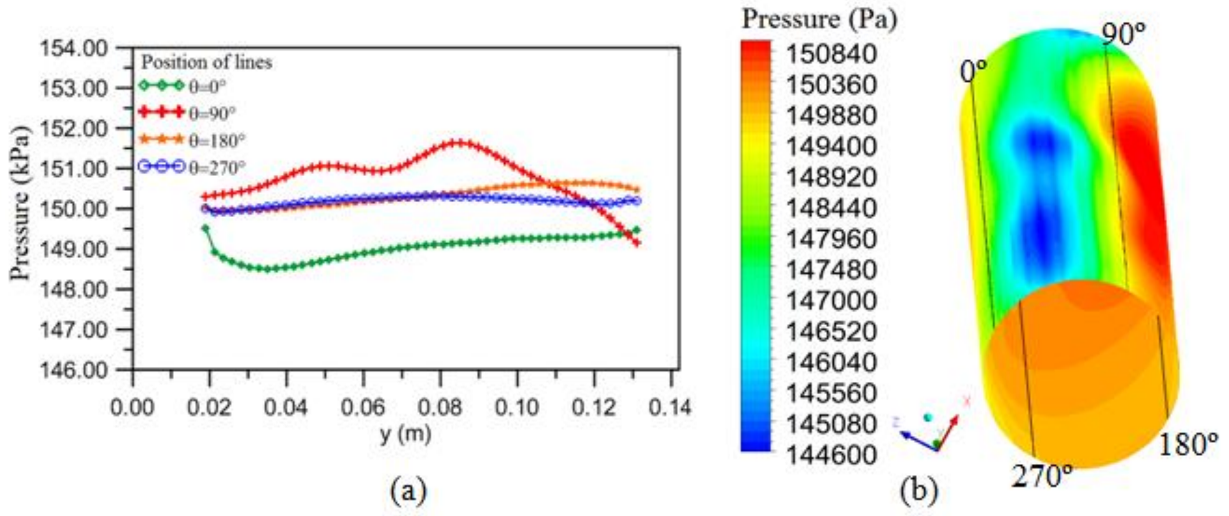

Figure 14. Pressure profiles (a) and pressure field (b) on the wall of membrane 4.

the velocity field near the membrane 2, Figure 15 (d), one can see an increase in the velocity of the flow approaching the membrane, which is due to the favorable pressure gradient, followed by a region of reduced velocity.

Figure 16 shows the distribution of oil concentration in shell-and-tubes module. In general, one can notice a higher oil concentration on the central faces of the module, corresponding to the region of lower flow velocity and, therefore, lower mass transfer, which makes this area more prone to oil accumulation. On the membrane surface facing the shell, one can observe a lower oil concentration, which is an effect of the increased flow velocity in this region and the consequent separation of the boundary layer with the formation of vortexes.

Figure 17 shows the concentration field evaluated at different transverse planes (A, B, and C) on the separation module. From the analysis of this figure one can see that the highest concentration gradient occurs in the region between the membranes as a consequence of the mixture hydrodynamic behavior around the tubular membranes. Some regions can be observed on planes A, B, and C where the concentration is close to the feed concentration (1.0 kg/m^3), mainly in the shell of the separation module. This fact is due to

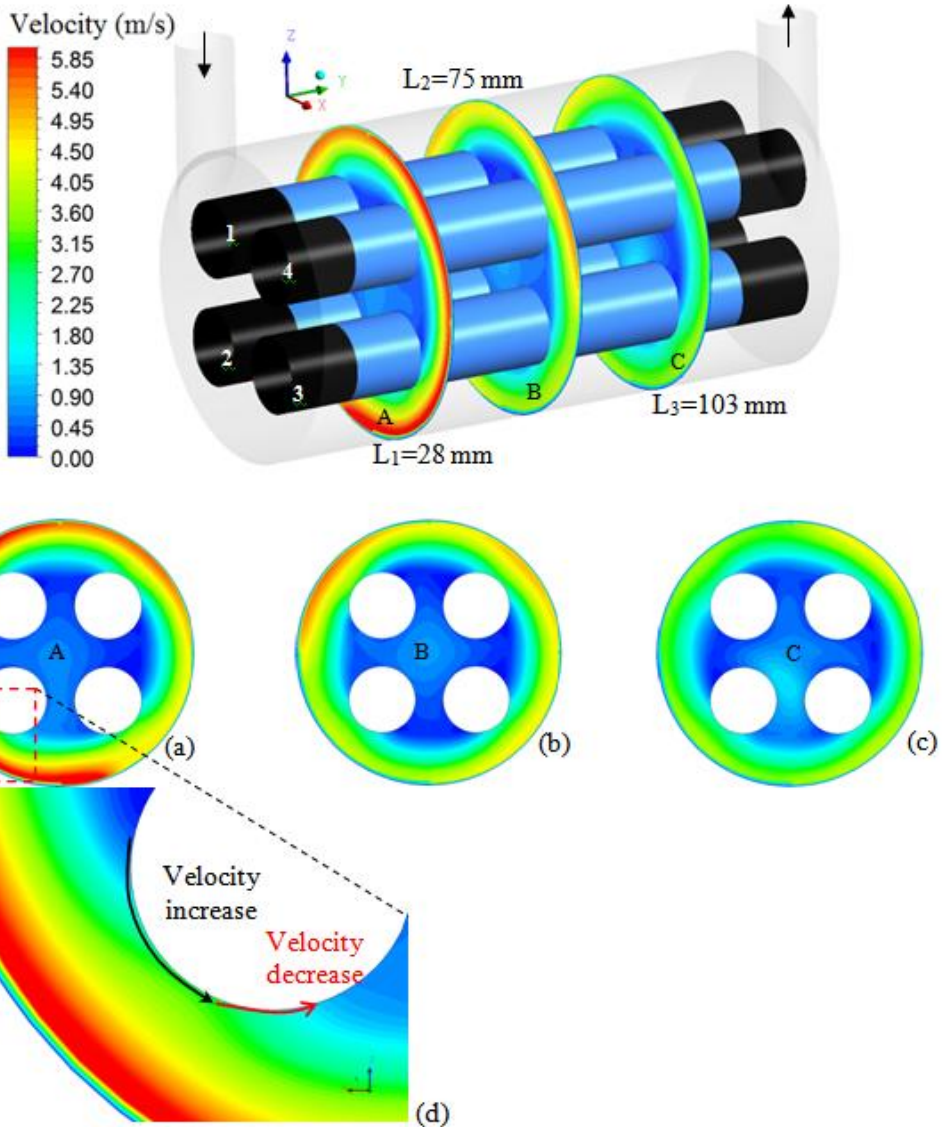

Figure 15. Velocity field on the transverse planes A, B, and C.

the different hydrodynamic characteristics of the flow induced by the tangential inlet, the action of the centrifugal force and the permeate flow, which favors the transport of oil particles toward the center of the module and next to the membrane surface.

Figure 18 illustrates the concentration distributions at the surface of the ceramic membrane as a function of the longitudinal position, *y*, in four angular positions 0°, 90°, 180°, and 270°, as originally illustrated in Figure 10. It is evident that the higher oil concentration on the surface of the membranes is located in the region between the membranes. In the angular position 0°, higher oil concentrations are found in

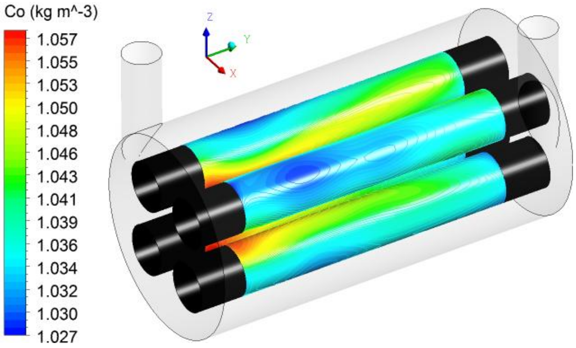

Figure 16. Distribution of oil concentration on the membrane wall.

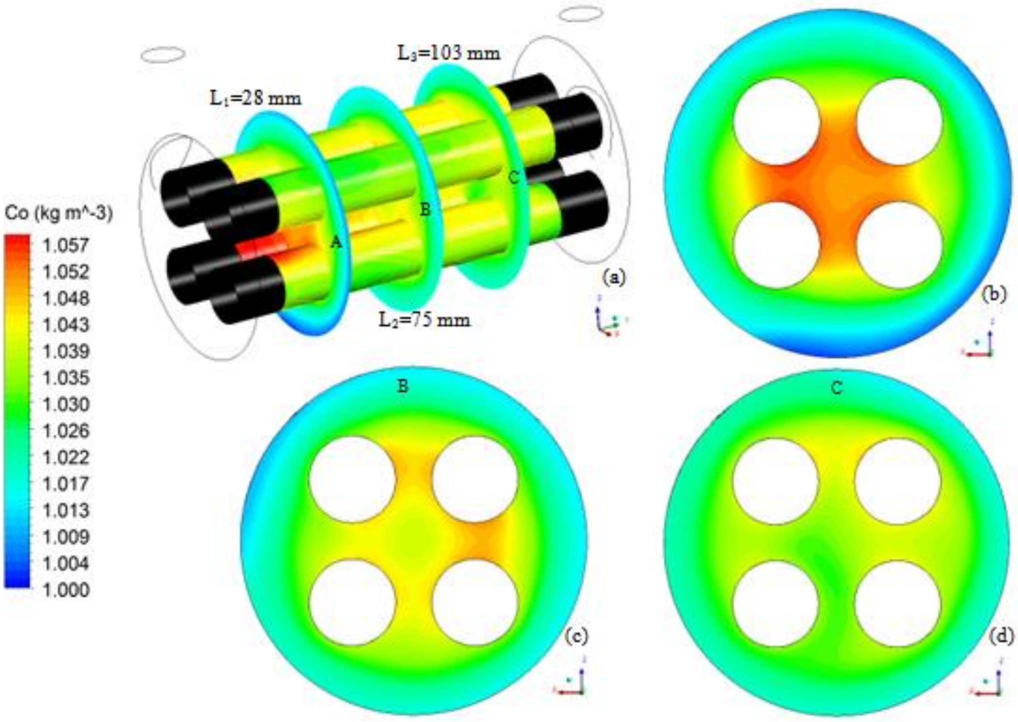

Figure 17. Oil concentration field on the membrane wall in the planes A, B, and C.

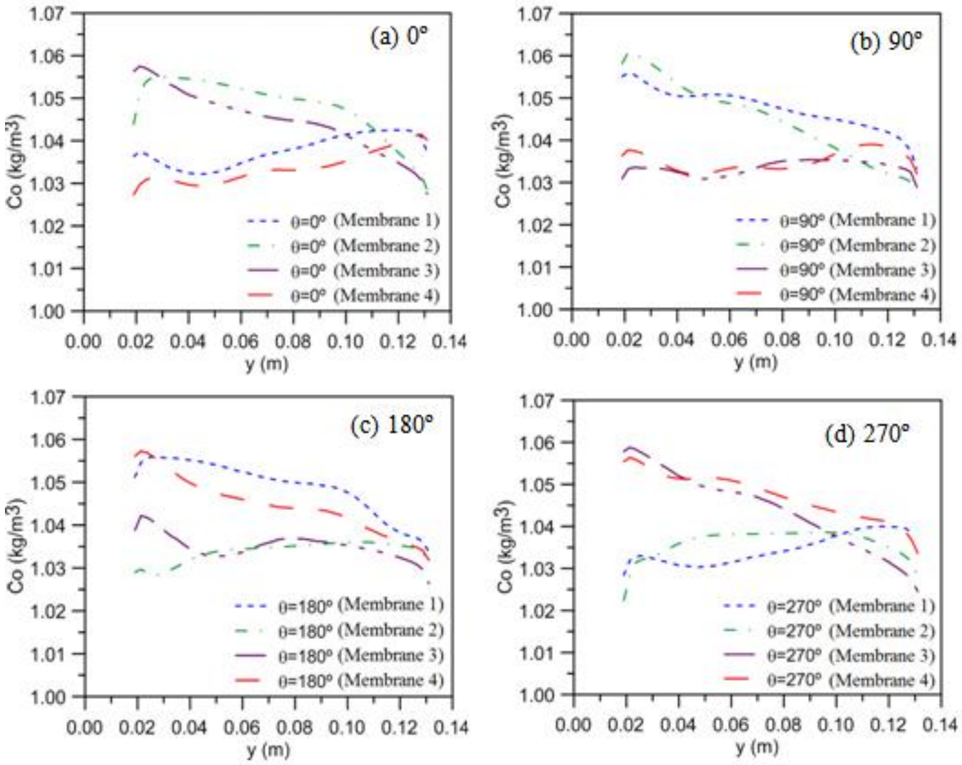

Figure 18. Oil concentration in the membrane wall as a function of the axial coordinate *y* in four angular positions.

membranes 2 and 3 (region between membranes); in the angular position 90°, the highest oil concentrations are found in membranes 1 and 2 (region between membranes); in the angular position 180°, higher oil concentrations are found in membranes 1 and 4 (region between membranes), and, finally, in the angular position 270°, membranes 3 and 4 have the highest oil

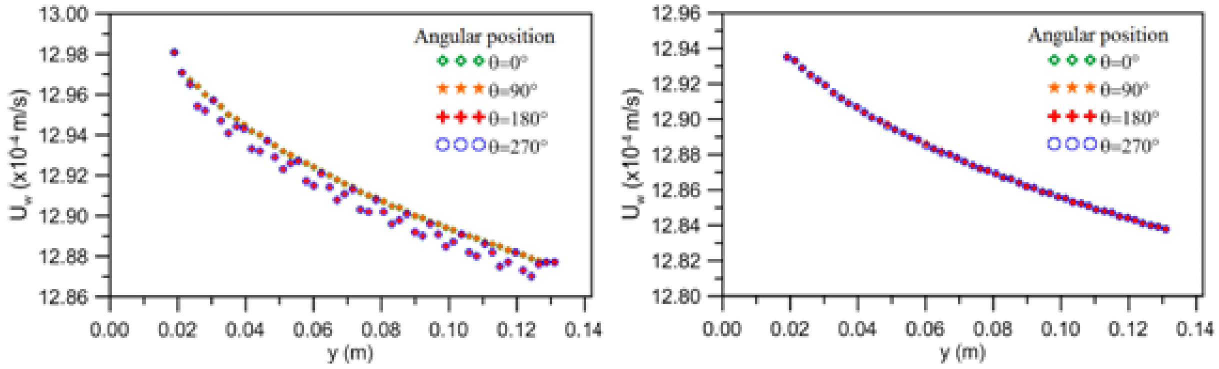

(a) Membrane 1 (b) Membrane 4

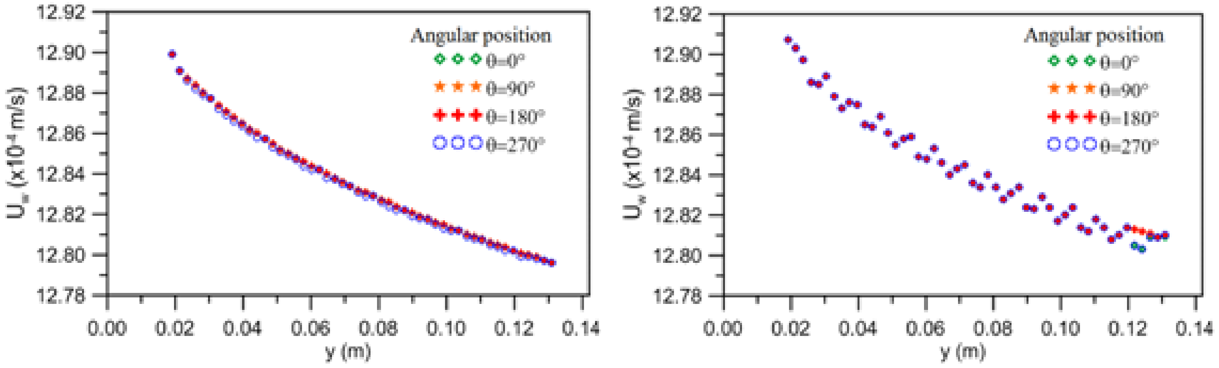

(c) Membrane 2 (d) Membrane 3

Figure 19. Permeate fluid velocity as function of the axial position at the surface of the membrane.

concentrations. In all cases, one can see that the oil concentration decreases in value along the membrane surface up to the outlet region.

In Figure 19, the distributions of permeate fluid velocity are illustrated as a function of the longitudinal positions, *y*, at the surface of the membrane in different angular positions (0, 90, 180, and 270°).

One can observe that membranes 1, 2, 3, and 4 presented average permeate velocities of 1.29 x 10^{-3}, 1.28 x 10^{-3}, 1.28 x 10^{-3}, and 1.28 x 10^{-3} m/s, respectively. In terms of permeate total mass flow rate, the shell-and-tubes module presented a permeate average flow of approximately 0.038 kg/s.

Cunha et al. (2014) studied the water/oil separation process using a porous membrane tube with the same properties of the porous media and of the fluid used in this work, with inner and tangential laminar flow, and Reynolds number of 1,000. The authors observed a permeate flow of 4.5 x 10^{-5} m/s, or mass flow of 3.17 x 10^{-5} kg/s. In the present work, the external flow with Reynolds number is equal to 3,820 under whirling regime presented a permeate flow 1,200 times higher. Although flow velocity had been higher, resulting in a higher driving force (transmembrane pressure) and favoring the permeate flow, it must be emphasize that the configuration of the separation module and the whirling flow favor the removal of oil from the surface of the membrane.

4. CONCLUSIONS

In this paper, it was explored the diffusion-convection phenomena in tubular membrane. Emphasis was given to ultrafiltration process and polarization concentration boundary layer. Interest in this type of problem is motivated by its importance in many practical situations related to fluid treatment. From the predicted results reported in this paper it can be conclude that:

The physical and geometrical parameters of the separation module affect directly the distribution of oil concentration in the module, the transmembrane pressure, and the permeation rate.

The reduction of the permeate flow is one of the main disadvantages of the use of porous membranes in the filtration process. The development of technologies capable of reducing the influence of the phenomena, and leading to a reduction of the permeate flow becomes necessary to enhance and expand this technique, which is more cost-effective and efficient compared to other separation methods.

ACKNOWLEDGEMENTS

The authors would like to express their gratitude to the Brazilian research agencies CNPq, CAPES, FINEP, ANP, and PETROBRAS for supporting this work and to the authors of the references cited in the paper, who helped to improve its quality.

5. REFERENCES

Agarwal, G.P.; Kaur, J. Studies on transmission in thin channel flow module: the role of dean vortices for improving mass transfer. **Journal of Membrane Science**, v. 188, p. 9-20, 2002.

Baker, R. W. **Membrane Technology and Applications**. California: John Wiley & Sons, 2004. 545p. https://doi.org/10.1002/0470020393

Belfort, G. Fluid mechanics in membrane filtration: recent developments. **Journal of Membrane Science**, v.40, p. 123-147, 1989. https://doi.org/10.1016/0376-7388(89)89001-5

Cunha, A. L.; Farias Neto, S. R.; Lima, A. G. B.; Barbosa, E. S.; Souza J. S. **Numerical study of the separation process through porous membranes**. In: XI Ibero-American Congress of Mechanical Engineering, 2013, La Plata, Argentina.

Cunha, A. L.; Souza J. S.; Farias Neto, S. R.; Lima, A. G. B.; Barbosa, E. S. Separation Process by Porous Membranes: A Numerical Investigation. **Advances in Mechanical Engineering**, v.2014, p. 1-9, 2014.

Damak, K.; Ayadi, A.; Schmitz, P.; Zeghmati, B. Modeling of cross-flow membrane separation processes under laminar flow conditions in tubular membrane. **Desalination**, v.168, p. 231-239, 2004a. https://doi.org/10.1016/j.desal.2004.07.003

Habert, A. C.; Borges, C. P.; Nobrega, R. **Separation Process Membrane. School of Chemical Engineering** - COPPE/UFRJ, 1ª Ed, e-papers, Rio de Janeiro, 2006.

Kulkarni, S. S.; Funk, E. W.; Li, N. N. Ultrafiltration. In: Winston Ho, W.S., Sirkar, K.K., Reinhold V.N. (Ed). New York: **Membrane Handbook**, p. 432-445, 1992.

Pak, A.; Mohammad, T.; Hosseinalipour, S.M.; Allahdinib, V. CFD modeling of porous membranes. **Desalination**, v.222, p. 482-488, 2008. https://doi.org/10.1016/j.desal.2007.01.152

Paris, J.; Guichardon, P.; Charbit, F. Transport phenomena in ultrafiltration: a new two-dimensional model compared with classical models. **Journal of Membrane Science**, v.207, p. 43-58, 2002. https://doi.org/10.1016/S0376-7388(01)00752-9

Song, L. Flux decline in crossflow microfiltration and ultrafiltration: mechanisms and modeling of membrane fouling. **Journal of Membrane Science**, v.139, p. 183-200, 1998. https://doi.org/10.1016/S0376-7388(97)00263-9

Yuanfa, L.; Gaohong, H.; Liu, X.; Xiao, G.; Baojun, L. CFD simulations of turbulent flow in baffle-filled membrane tubes. **Separation and Purification Technology**, v.67, p.14-20, 2009. https://doi.org/10.1016/j.seppur.2009.02.022

Vieira, T. M.; Souza, J. S.; Barbosa, E. S.; Cunha, A. L.; Farias Neto, S. R.; Lima, A. G. B., Numerical study of oil/water separation by ceramic membranes in the presence of turbulent flow. **Advances in Chemical Engineering and Science**, v.2, p. 257-265, 2012. https://doi.org/10.4236/aces.2012.22030

Zimmerer, C. C., Kottke, V. Effects of spacer geometry on pressure drop, mass transfer, mixing behavior and residence time distribution. **Desalination**, v.104, p.129-134, 1996. https://doi.org/10.1016/0011-9164(96)00035-5